



Contents lists available at ScienceDirect

European Journal of Medicinal Chemistry

journal homepage: <http://www.elsevier.com/locate/ejmech>

Research paper

Isoquinoline-based biaryls as a robust scaffold for microtubule inhibitors

Yvonne Kraus¹, Carina Glas¹, Benedikt Melzer, Li Gao, Constanze Heise, Monique Preuße, Julia Ahlfeld, Franz Bracher, Oliver Thorn-Seshold*

Department of Pharmacy – Center for Drug Research, Ludwig-Maximilians University of Munich, Butenandtstrasse 5-13, Munich, 81377, Germany

ARTICLE INFO

Article history:

Received 9 August 2019

Received in revised form

8 October 2019

Accepted 6 November 2019

Available online xxx

Keywords:

Colchicine

Cytoskeleton

Isoquinoline

Microtubule dynamics

Tubulin polymerisation inhibitor

ABSTRACT

We here report the discovery of isoquinoline-based biaryls as a new scaffold for colchicine domain tubulin inhibitors. Colchicinoid inhibitors offer highly desirable cytotoxic and vascular disrupting bioactivities, but their further development requires improving *in vivo* robustness and tolerability: properties that both depend on the scaffold structure employed. We have developed isoquinoline-based biaryls as a novel scaffold for high-potency tubulin inhibitors, with excellent robustness, druglikeness, and facile late-stage structural diversification, accessible through a tolerant synthetic route. We confirmed their bioactivity mechanism *in vitro*, developed soluble prodrugs, and established safe *in vivo* dosing in mice. By addressing several problems facing the current families of inhibitors, we expect that this new scaffold will find a range of *in vivo* applications towards translational use in cancer therapy.

© 2019 Elsevier Masson SAS. All rights reserved.

1. Introduction

The protein tubulin is a prime target for development of cancer therapeutic inhibitors, most famously since the microtubule cytoskeleton it forms plays a crucial role in mitosis, which is required for the progression of all cancer types [1,2]. Tubulin-inhibiting Antimitotic cytotoxins from the classes of taxanes and of vinca alkaloids have become blockbuster drugs, and have been used in the treatment of millions of patients [3]. A third class of tubulin inhibitors are the colchicine domain inhibitors (CDIs). CDIs with low- or sub-nanomolar antiproliferative/cytotoxic activity *in cellulo* have been extensively developed. However, *in vivo* their main bioactive mechanism at tolerated doses is not cytotoxicity mediated through tubulin disruption in target (tumour) cells, but instead vascular disrupting agent (VDA) activity, mediated by disrupting microtubule integrity in the endothelial cells lining the vascular system. In the tumour neovascular network this disruption is poorly withstood, leading to stanching of tumoural blood flow and necrosis of the tumour interior [4]. VDA activity is thus highly desirable as a complementary mechanism to typical cytotoxins that usually

target the tumour exterior but are poorly effective in the interior [5].

The prototypical requirements for CDI bioactivity have been well studied [6]. CDIs typically display pharmacophore-relevant groups on two aryl rings, here denoted as north and south rings, that are usually twisted with respect to one another [7]. The south ring typically features a 3,4,5-trimethoxy substitution pattern and the north ring a monomethoxy substituent with a hydrogen or an optional small polar group (OH, NH₂, F) in the *ortho* position [8,9]. These substituents ensure potent binding to tubulin when correctly arranged on the scaffold “exterior”. Combretastatin A-4 (**CA4**; Fig. 1a) [10] illustrates these features. It is a *Z*-stilbene that acts as a low nanomolar cytotoxin *in cellulo*, and its *E*-isomer - whose methoxy groups do not project in the correct directions - is several orders of magnitude less bioactive [11].

A crucial result observed during CDI development is that although *in cellulo* a broad range of scaffold “interiors” for CDIs can deliver good cytotoxic potency as long as the “exterior” substituents are correctly arranged, *in vivo* the scaffold choice often determines medicinal chemistry factors critical for therapeutic applications. For example, **CA4** reached Phase III clinical trials as a VDA in the form of its phosphate prodrug **CA4P**, while colchicine (which has a similar disposition of substituents and similar *in cellulo* potency) is not tolerated at the doses required for VDA activity (Fig. 1a) [12,13]. Typical scaffold-dependent factors decisive for

* Corresponding author.

E-mail address: oliver.thorn-seshold@cup.lmu.de (O. Thorn-Seshold).

¹ These authors contributed equally to this work.

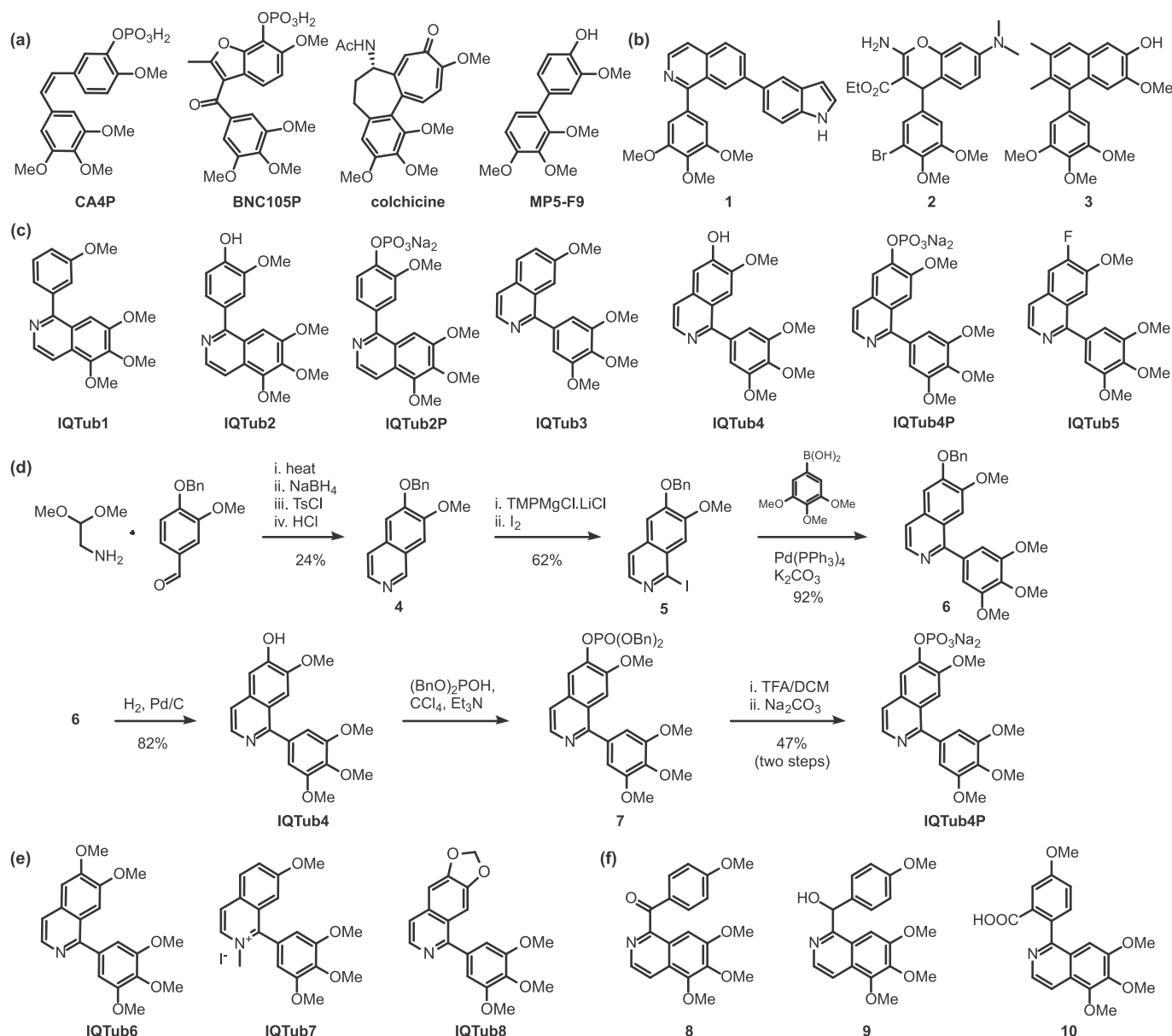


Fig. 1. (a) Archetypal literature-known CDIs. (b) Selected literature-reported biaryl-type CDIs. (c) IQTubs and their prodrugs. (d) Synthetic route to IQTubs, shown exemplarily for IQTub4 and IQTub4P. Ts: *para*-toluenesulfonyl, TMP: 2,2,6,6-tetramethylpiperidiny, Bn: benzyl, TFA: trifluoroacetic acid. (e,f) Control IQTubs, and other control compounds similar to IQTubs, used in this study (IQTub6[29], IQTub8[30], 8 and 9[31], and 10[32]) were previously reported but not biologically evaluated.

in vivo use include robustness to spontaneous deactivation *in vivo* (e.g. stilbenes suffer *cis* to *trans* isomerisation [14]), as well as traditional ADME/PK parameters including metabolism (e.g. cytochrome degradation of, or inhibition by, the stilbene double bond [15,16], or metabolic processing of aryl aryl ketone bridges [17,18]) and overall plasma residence time [14], as well as their ease of synthetic access.

CA4-inspired CDIs with north and south rings held at a twist are the class of CDI VDAs which has progressed furthest in clinical trials, and these have been excellently reviewed [6,7,13]. A variety of such scaffolds have been tested, aiming to improve upon the *in vivo* properties of CA4P. Beyond stilbenes (like CA4P analogues CA1P [19] and AVE8062[20]), colchicinoids such as ZD6126 [21], aryl aryl ketones such as BNC105P [22], and a range of other scaffolds have been used for CDIs, several of which feature *in vivo*-confirmed VDA activity (Fig. 1a) [4]. Other classes of CDIs, such as the quasi-planar

indanocine, plinabulin, nocodazole and indanorin [13], are less developed for *in vivo* applications and generally have not been confirmed to display VDA activity. Improved techniques for screening for VDA activity [23] are currently opening new perspectives for VDA development. While no CDIs have yet been approved as VDAs [24], the value of investigating new CDI scaffolds with potentially improved VDA activity has been elegantly stated by Fojo [25]; we here report our progress in this area [26].

2. Results

Design and Synthesis. We primarily desired to develop CA4-inspired CDIs with VDA potential, featuring a molecular scaffold that would be highly robust to *in vivo* inactivation and/or metabolic degradation mechanisms that affect the major VDA scaffolds in clinical trials (stilbenes and aryl aryl ketones). By contrast to the

range of twisted bis-aryl structures with one- or two-atom bridging groups between the rings (e.g. **BNC105P** or **CA4P**, respectively) and the CDIs with non-aromatic bicyclic rings (e.g. dihydronaphthalenes, benzosuberones, benzodiazepines) [6,27,28], we found that fully aromatic biaryls are sparsely reported and underexplored as CDIs. This presented an opportunity, as a biaryl bond promises to be more metabolically resistant than other bridging bond types; biaryls can be druglike and do not require stereospecific synthesis; a biaryl is permanently in a ring-twisted state that is usually crucial for CDI bioactivity [6] (in contrast to stilbenes that can isomerise to a planar state); and biaryls can be constructed by easily diversifiable late-stage cross-couplings. Motivated by similar logic, a very limited number of CDI biphenyls such as **MP5-F9** [14] have previously been developed (Fig. 1a), but their potency was approximately 500-fold less than of the cognate stilbene-type CDIs and as far as we are aware they were unfavourable for further development. Alternatively, Miller et al. [17,18] reported a series of triaryl CDIs (e.g. **1**; Fig. 1b). However, we considered that triaryl designs introduce undesirable synthetic complexity and molecular weight, and they do not promise solubility high enough for *in vivo* application (typically, > 10 mM injection concentration in aqueous media for small animal studies). We therefore determined to explore biaryls that occupy similar space to colchicine itself, i.e. that feature one bicyclic and one monocyclic aromatic ring, in the hope that this would allow high potency, good solubilisation, and minimal complexity in our designs.

It was not obvious whether the north or the south ring inside the CDI pharmacophore would be more suitable for replacement by such a bicyclic aromatic ring. Cell-active CDIs with a large north ring are well attested (e.g. **2** and **3**; Fig. 1b) but the south ring has also been reported to tolerate replacement with bicyclics [13], which our recent experience [33–35] has supported. We therefore determined to synthesise and evaluate both “south” and “north” ring replacement types. We focused on isoquinolines as the bicyclic ring (rather than e.g. naphthalenes) due to isoquinolines’ straightforward and flexible retrosynthesis, as well as the solubility enhancement expected from including a ring nitrogen. Within the south and north sets we also wanted to explore both hydrogen and small polar group substituents at the variable position. This ligand-based design process yielded south ring replacements **IQTub1-2** and north ring replacements **IQTub3-5**. According to established SAR [7,13] we desired that **IQTub2** and/or **IQTub4** would prove the most potent members of their sets, according to preference of the isoquinoline for occupying the south or the north position. To render them potentially *in vivo* suitable we also designed their phosphate prodrugs **IQTub2P/IQTub4P** (Fig. 1c). The phenolic phosphate prodrug strategy has been particularly successful for CDI VDAs (**CA4P** and **CA1P** [36], **ZD6126** [21], **BNC105P**²²) in conferring suitable water-solubility for *in vivo* application (allows i.v. injection at high concentration in aqueous media [22] and reduces plasma protein binding compared to the otherwise lipophilic phenols [21]) [13]. Although the phosphates are not cell permeable they can be efficiently and nonspecifically cleaved extracellularly by diverse phosphatases to liberate the active, membrane-permeable phenols which diffuse passively across membranes to exert bioactivity by binding to tubulin at the lipophilic colchicine binding domain [37].

Noting that a CDI’s bioactivity is typically abolished if its variable position is not occupied by small groups (but instead by OMe, Et, etc) [13], we designed *O*-methylated **IQTub6** in the hope it would be inactive (a “designed-inactive” control [33,34]). This probes whether **IQTubs** reproduce the general CDI structure-activity relationship (SAR): if so, it would support the conjecture that **IQTubs** are also CDIs. To explore other polarity-altering alkylations, we also designed *N*-methylated quaternary **IQTub7** and benzo-dioxolo **IQTub8**, to extend our SAR in case the north ring

replacements proved bioactive (Fig. 1e). Searching the literature across a similar scaffold space showed that only **IQTub6**, first reported in the 1930s [29] as a papaverine analogue, and **IQTub8**, reported by Reeve and Eareckson in 1950 [30] during a study towards di- and tetrahydroisoquinoline analogues of podophylotoxin, had previously been reported. However neither of these compounds had been evaluated for bioactivity nor were they used in SAR studies, so we determined to test them ourselves (see below and Supporting Information).

The isoquinoline building blocks were synthesised by a modified Pomeranz-Fritsch reaction according to Reimann [38]. These were directly metalated at C-1 using Knochel-Hauser base [39] similarly to a published procedure [31], and Suzuki coupled with appropriately-substituted phenylboronic esters [32], delivering the targets **IQTub1-5** and **IQTub8** after optional deprotection. Methylating **IQTub3** and **IQTub4** yielded **IQTub7** and **IQTub6** respectively. This synthetic protocol is tolerant to a range of substituents, and allows late-stage diversification from a given isoquinoline scaffold with high overall yields (Fig. 1d and Supporting Information). All **IQTubs** were then taken into cell biological testing for antiproliferative activity, using the resazurin viability assay in HeLa cervical cancer cell line [40].

Structure-activity studies of IQTubs. Neither of the south ring replacements showed strong cytotoxicity (apparent EC₅₀s: **IQTub1** ~ 15 μM, **IQTub2** ~ 50 μM). We controlled in two orthogonal ways whether re-orientation of the substituents could permit bioactivity while still retaining the south ring replacement strategy. Firstly, noting that ketone-bridged compounds such as **BNC105P** (Fig. 1a) and phenstatin [13] are potent CDIs, we slightly increased the flexibility between the aromatic rings by introducing a one-atom bridge to allow subtle changes in relative ring orientation while maintaining the positioning of all methoxy groups - an attested strategy in VDA development [6]. To this end we tested ketone bridged alkaloid thalimicrinone (**8**) as well as its *sp* [3]-configured carbinol synthetic precursor **9** [31] (Fig. 1e), however, neither was bioactive in our hands (EC₅₀ > 80 μM). Next, we reoriented the north ring methoxy group from the *meta* into the *para* position, in case a larger bite angle between the south and north ring methoxy substituents would be better accommodated. For this we examined oxoisoaporphine precursor **10** from previous work [32] (Fig. 1e), but this too was inactive in our hands (EC₅₀ > 100 μM). We concluded that south ring replacement with the isoquinoline was not viable.

Pleasingly though, the designed-active north ring replacements **IQTub3-5** showed strong bioactivity with cellular cytotoxicity EC₅₀ values in the mid-nanomolar range (Fig. 2a). As hoped, the designed-inactive *O*-methylated control compound **IQTub6** was indeed inactive (EC₅₀ > 20 μM), suggesting that the north ring replacement **IQTubs** obey the SAR expected for colchicine site binders. We found no literature precedence for expecting either activity or inactivity of charged compound **IQTub7**, but in the event it was inactive (EC₅₀ > 30 μM). Previously reported structure **IQTub8** (see also discussion in Supporting Information) [30] featuring a benzodioxole north ring - which could be able to bind similarly to isovanillyl **IQTub4** according to literature SAR [13] - proved inactive in our hands (EC₅₀ > 20 μM; Fig. 2b).

However, as we observed turbidity while handling **IQTub8**, we assumed that its apparent cellular bioactivity could have been limited by poor solubility. We were therefore motivated to cross-check whether water-soluble prodrugs of both scaffold orientations would support our choice of the north ring strategy and confirm the inactivity of the south ring type. We synthesised phenolic phosphate prodrug **IQTub4P**, which was soluble in aqueous buffer to >10 mM (see Supporting Information). It displayed near-identical cytotoxicity in cell culture as its free phenol form **IQTub4** (Fig. 2) indicating that *O*-phosphorylation is reliable as a strategy for

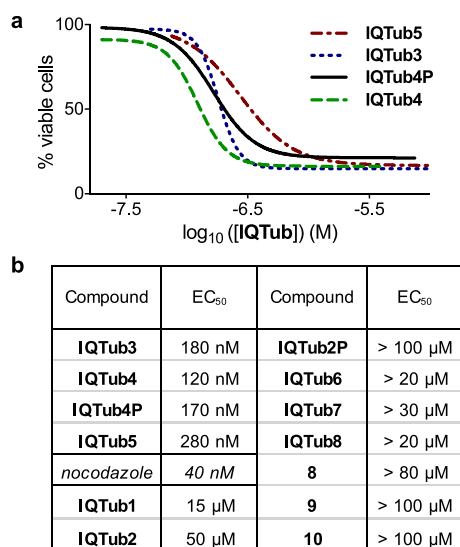


Fig. 2. Cell viability assessment of IQTubs. (a) Antiproliferation assays showed strong dose-dependent cytotoxicity for north ring designs IQTub3, IQTub4, IQTub4P and IQTub5 (one representative experiment of three independent experiments shown). (b) EC₅₀ values for the bioactive compounds and permutation controls, as well as reference compound nocodazole. (HeLa cell line; 48 h incubation; resazurin assays; see also Supporting Information).

soluble prodrugs (see below); comparison of both compounds' cytotoxicities in a second cell line (HL-60 human leukaemia line) confirmed both their mid-nanomolar bioactivity and their close correspondence of potency (EC₅₀s in HL-60: IQTub4: 340 nM, IQTub4P: 570 nM). To check whether IQTub1-2's bioactivity could have been undercut by poor solubility, we synthesised phosphate prodrug IQTub2P, but its cytotoxic activity was not measurable (EC₅₀ >> 100 μM). We concluded that neither solubility nor substituent orientation effects had obscured the cytotoxicity of IQTub1-2, and that the isoquinoline is not well-tolerated as a south ring replacement. We attributed the weak apparent antiproliferative activity of the "inactive" IQTubs (e.g. IQTub1, IQTub6) as tubulin-independent aggregation-dependent effects, known for similar motifs [9,33], and confirmed this in mechanistic studies (see below).

With their bioactivity matching our SAR understanding, we considered that north ring replacement IQTubs were a viable approach to a new scaffold for CDIs, and we determined to proceed with the potent and well-soluble IQTub4P.

Drug-relevant properties of lead IQTub4/IQTub4P. We then measured selected parameters of IQTub4P that would be relevant for *in vivo* applications of the isoquinoline-based biaryl (using IQTub4 in these assays since it should be the *in situ*-dephosphorylated IQTub4 that penetrates into cells to reach its site of action [13]). By examining its compound stability in the presence of mouse and human liver microsomes, we concluded that IQTub4 has good metabolic stability (Fig. 3a). Studies with the five major human cytochrome P450s showed no significant inhibition of these CYPs by IQTub4, indicating that it may escape typical drug-drug interaction pathways (Fig. 3b). A fluorescence polarisation reporter assay for hERG channel inhibition showed no significant effect at the highest tested concentration (Fig. 3c). Lastly, we experimentally determined the distribution coefficient logD at pH 7.4 to be 2.18, which is within a range (1–3) considered optimum for general *in vivo* use [41]. These results suggested that IQTub4 was suited for further pharmacological evaluation (see Supporting Information for further details and assay benchmarking).

IQTubs inhibit microtubule structure and function. We next

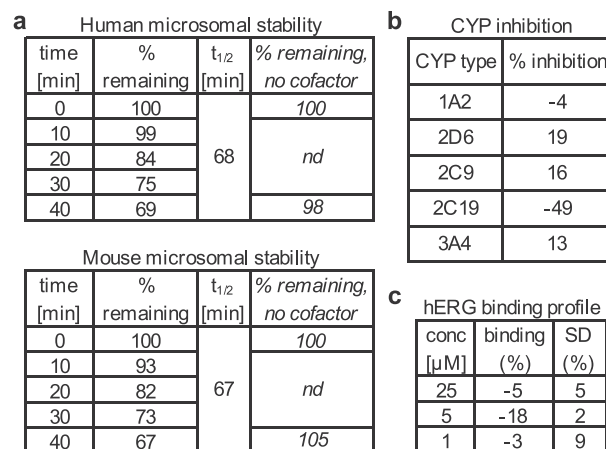


Fig. 3. Drug property assessments of IQTub4. (a) Metabolic stability against mouse and human liver microsomes (IQTub4 at 2 μM). (b) Inhibition assay against five human cytochrome P450s (IQTub4 at 10 μM). (c) hERG channel inhibition assay.

moved to confirm whether the cytotoxic IQTubs' mechanism of action was indeed inhibition of tubulin polymerisation. We first visualised their capacity for microtubule (MT) network perturbation in cell culture. Sustained tubulin polymerisation inhibition disorganises and ultimately depolymerises cellular MT networks. We observed dose-dependent MT network depolymerisation with the active IQTubs (Fig. 4a and b), and z-stack projection images additionally revealed that cells treated with low doses of active IQTubs already accumulated into rounded, mitotically arrested states with defective spindles and chromosome alignments (Fig. 4c). These are hallmarks of treatment with MT-depolymerising agents. In contrast, neither designed-inactive SAR control IQTub6 (Fig. 4a) nor non-cytotoxic IQTub7-8 (Fig. S5) gave any MT disorganisation in this assay even at the highest tested concentrations, suggesting that the bioactivity observed for IQTubs is tubulin-specific.

The cytotoxic effects of CDIs *in cellulo* typically arise due to interruption of tubulin reorganisation in the mitotic spindle, which blocks mitosis, ultimately triggering cell death (as observed under longer-term treatments in the viability assays). If IQTubs' tubulin-disrupting effects were indeed the cause of their observed cytotoxicity, treated cells should be measurably arrested in G2/M-phase. We therefore used flow cytometry to perform cell cycle analysis of HeLa cells under IQTub4P treatment. Results indeed showed extensive G2/M-arrest from concentrations as low as 500 nM (Fig. 5a).

IQTubs inhibit tubulin polymerisation dynamics. Aiming to confirm the molecular mechanism of IQTub bioactivity as one of direct binding to tubulin (rather than binding to regulatory proteins or affecting signalling), we then tested for inhibition of tubulin polymerisation dynamics in cell-free settings using purified tubulin. We observed closely similar polymerisation inhibiting activity for IQTubs as for colchicine itself, which strongly supported the direct binding interpretation and the mechanistic classification of the IQTubs as microtubule depolymerisers (Fig. 5b).

Inhibition of tubulin polymerisation dynamics was then directly assayed *in cellulo* by live-cell confocal video microscopy in HeLa cells transfected to express EB3-YFP fusion protein. EB3-YFP is a fluorescent marker that selectively labels the growing tips of microtubules and manifests as moving "comets" when MTs are growing; the comets stop and disappear upon inhibition of tubulin polymerisation [9]. Within 2 min of applying prodrug IQTub4P, cellular EB3 comets stopped and vanished, indicating that extracellular dephosphorylation to IQTub4 followed by internalisation

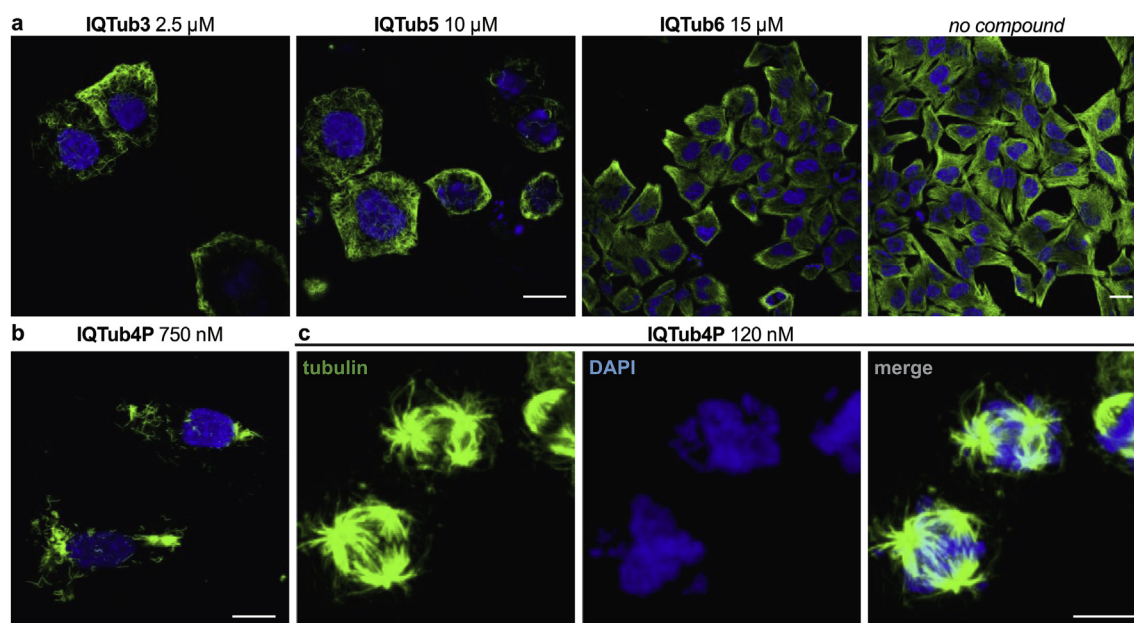


Fig. 4. Confocal microscopy assessment of cellular microtubule networks after treatment with **IQTubs**. (a) **IQTub3** and **IQTub5** induce MT network breakdown (panels on same scale) while SAR control **IQTub6** does not alter MT network integrity (compare to untreated control; panels on same scale). (b) Prodrug **IQTub4P** is active *in cellulo* at submicromolar doses. (c) 120 nM **IQTub4P** already leads to mitotic arrests and the formation of aberrant multipolar spindles (tubulin panel) with resulting unstructured chromosome alignment (DAPI panel). Maximum intensity projection along the z-axis of an image stack. (HeLa cells, 24 h treatment, green: α -tubulin stain for microtubule polymer network, blue: DAPI nuclear counterstain, all scale bars 20 μ m; see also Fig. S5). (For interpretation of the references to colour in this figure legend, the reader is referred to the Web version of this article.)

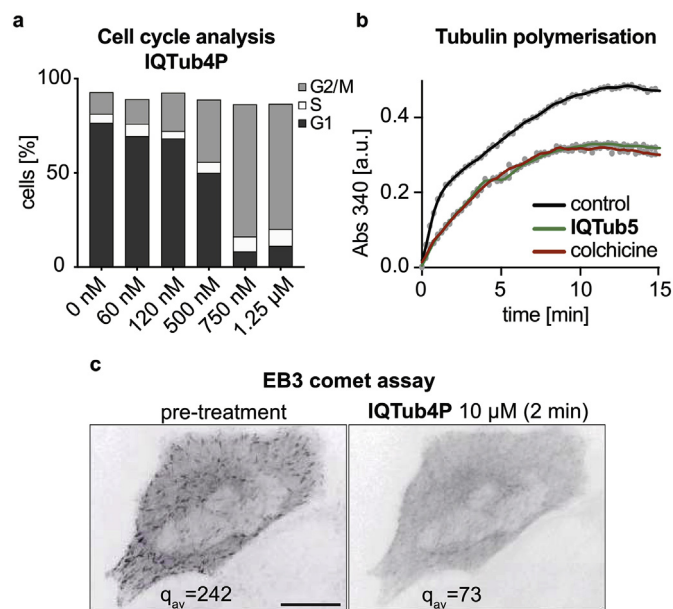


Fig. 5. (a) Cell cycle analysis of **IQTub4P**-treated cells shows potent induction of G2/M arrest. (b) **IQTub5** inhibits tubulin polymerisation (cell-free) with similar potency to the reference tubulin inhibitor colchicine (turbidimetric assay; **IQTub5** at 20 μ M, colchicine at 16 μ M). (c) Imaging of MT polymerisation dynamics in live HeLa cells transfected with EB3-YFP. EB3 comets were tracked, before and then 2 min after treatment with 10 μ M **IQTub4P** (comet tails tinged purple, tips shown black); EB3 comet count (q) statistics were averaged over 7 cells (see Supporting Information for details).

rapidly gives potent inhibition of cellular tubulin polymerisation dynamics (Fig. 5c).

IQTubs are well-tolerated *in vivo*. These assays offered several independent indications that **IQTubs** are potent, robust

microtubule depolymerisers with SAR and performance matching expectations of CDIs. We considered this promising for their potential for *in vivo* performance, ultimately aiming at development of **IQTubs** as a new CDI VDA scaffold. To finish this early compound development study, we therefore assessed safe dosing parameters of **IQTub4P** *in vivo* in male and female Balb/c mice. Dose-escalation studies (i.p. and i.v. administration routes) established a single-administration maximal tolerated dose of 32 mg/kg (i.p.) and 50 mg/kg (i.v.). Repeated dosing (3 administrations, 48 h intervals) were conducted with 25 mg/kg for both i.v. and i.p. routes and were tolerated, thus **IQTubs** may avoid short-term cumulative toxicity, which is known for the most promising CDI VDAs. We consider these results favourable for further *in vivo* progress of this new scaffold; by comparison the archetypal CDI colchicine has a murine maximal tolerated dose around only 1 mg/kg [20].

3. Discussion and conclusion

The success of the taxanes and vinca alkaloids in clinical oncology has stimulated intense interest in novel tubulin inhibitors. Colchicine domain inhibitors offer a biological activity profile which not only includes the antimetabolic and pro-apoptotic effects common to all tubulin inhibitors, but also vascular disrupting effects that are highly desirable for cancer treatment. This has stimulated much research and development of CDIs and several have reached late-stage clinical trials for cancer treatment, although none have yet reached clinical approval.

Here we have performed ligand-based design of isoquinoline-based biaryls – a simple and robust chemical backbone – as new scaffolds for potent CDIs. These **IQTubs** are easily accessible with straightforward late-stage diversification using short, high-yielding synthetic routes; and they have shown excellent performance in early measurements of *in vivo*-relevant druglike properties. They display high cellular potency in long-term cellular studies as well as in short-term live-cell imaging. They deliver robustness to the

scaffold-specific spontaneous deactivation mechanism affecting stilbene CDIs as well as metabolic liabilities of other major CDI families, thus offering potentially advantageous ADME/PK compared to the current CDIs. Through SAR studies as well as extensive cellular and cell-free assays, we have clarified and supported their mechanism of action, showing multiple proofs that their tubulin inhibition matches the bioactivity expected for CDIs. Lastly, we have determined the *in vivo* tolerability for the lead compound **IQTub4P** to be more than an order of magnitude higher than that of the archetypal CDI colchicine, which is promising for future research into the *in vivo* applications and VDA performance of this potent, biologically robust IQT scaffold.

It should also be noted that VDAs are typically designed for short plasma residence times (with high dose tolerance), enabling fast but transient dose delivery to vascular endothelial cells, aiming that in this way only the more susceptible tumour neovasculature should lose microtubule-based mechanostasis during the time of exposure, therefore giving tumour-selective vascular shutdown [24,42]. In this context, the speed of dephosphorylation-internalisation-inhibition observed with **IQTub4P** (Fig. 5c) is particularly encouraging.

The current **IQTubs** already feature satisfying cellular potency, but we fully expect that ongoing SAR studies will deliver analogues with higher potency and/or significantly tuned biochemical properties. Still, their therapeutic performance cannot yet be predicted since cellular potency is known not to be the limiting factor for CDI VDA activity *in vivo*. Cardiotoxicity is a major dose- and therapy-limiting parameter with CDIs, which is known to be scaffold-dependent in that it is strongly affected by ADME/PK as well as molecular structural parameters [24]. In this context, enabling exploration of a new scaffold class with the potential for strongly differentiated ADME/PK and scaffold-dependent tolerability is a valuable step for the development of CDI VDAs and investigations of these parameters are ongoing.

The ease and substituent tolerance of **IQTub** synthesis is another important feature of this work, comparing favourably with many CDI scaffold systems. However, more broadly, we consider that the design logic of scaffold hopping from stilbene to isoquinoline-based biaryl scaffolds to improve *in vivo*-relevant drug properties is an exciting advance, promising medicinal chemistry applications to targets well beyond the current CDIs.

In closing, we predict that by unlocking isoquinoline-based biaryl tubulin inhibitors, this research will open up new possibilities for refinement of tubulin inhibitors, for *in vivo* VDA development, and for broader applications of robust biaryl designs to other pharmacophores.

4. Experimental section

Full and detailed chemical and biological protocols can be found in the Supporting Information.

Compound synthesis and characterisation. All reactions were performed with unpurified, undried, non-degassed solvents and reagents from commercial suppliers (Sigma-Aldrich, TCI Europe, Fisher Scientific etc.), used as obtained, under closed air atmosphere without special precautions, unless otherwise described. Manual flash column chromatography was performed on Merck silica gel Si-60 (40–63 μm). MPLC flash column chromatography was performed on a Biotage Isolera Spektra system, using Biotage prepacked silica cartridges. Thin-layer chromatography (TLC) was run on 0.25 mm Merck silica gel plates (60, F-254), with visualisation under UV light (254 nm and 365 nm). NMR characterisation was performed by ^1H and ^{13}C NMR spectra recorded on an Avance III HD 400 MHz Bruker BioSpin and Avance III HD 500 MHz Bruker BioSpin (^1H : 400 MHz and 500 MHz, ^{13}C : 101 MHz and 126 MHz).

HRMS was performed by electron impact (EI) at 70 eV (Thermo Finnigan MAT 95 or Jeol GCmate II spectrometers) unless stated otherwise. HPLC-MS: Analytical measurements for determination of the purities of the final products were performed on an Agilent 1100 SL coupled HPLC-MS system with $\text{H}_2\text{O}:\text{MeCN}$ eluent gradients through a Thermo Scientific Hypersil GOLD™ C18 column (1.9 μm ; $3 \times 50 \text{ mm}$) maintained at 25 °C, detected on an Agilent 1100 series diode array detector and a Bruker Daltonics HCT-Ultra spectrometer (ESI mode, unit m/z). Full experimental details are given in the Supporting Information.

4.1. Representative synthesis: **IQTub4**

6-Benzyloxy-7-methoxyisoquinoline (4) (first reported by a different procedure [43]). 4-Benzyloxy-3-methoxybenzaldehyde (4.99 g, 20.6 mmol) was dissolved in toluene (50 mL) and aminoacetaldehyde dimethyl acetal (2.38 g, 22.7 mmol) was added. Using a Dean-Stark apparatus the reaction mixture was heated to reflux for 16 h. After cooling to room temperature the volatiles were evaporated and the crude redissolved in MeOH (100 mL). The mixture was cooled to 0 °C and NaBH_4 (1.56 g, 41.2 mmol) was added portionwise over 30 min, then the reaction mixture was warmed to room temperature and stirred for 4 h. The volatiles were evaporated and the crude taken up in water (100 mL) then extracted with DCM ($3 \times 100 \text{ mL}$). The combined organic layers were dried over Na_2SO_4 , filtered and concentrated. The crude product was redissolved in DCM (100 mL) and NaOH (1.40 g, 35.0 mmol) and tetrabutylammonium hydrogensulfate (0.490 g, 1.44 mmol) were added. After stirring for 10 min at room temperature a solution of *p*-toluenesulfonyl chloride (4.71 g, 24.7 mmol) in DCM (60 mL) was added dropwise over 1 h. The reaction mixture was stirred for an additional hour. Water (100 mL) was added, phases were separated, the organic phase washed with water ($2 \times 100 \text{ mL}$) and brine (100 mL), dried over Na_2SO_4 and concentrated. The resulting crude product was dissolved in 1,4-dioxane (150 mL), aq. 6 M HCl (30 mL) was added and the reaction mixture heated to reflux for 16 h. After cooling to room temperature, the solution was poured into water (150 mL) and washed with diethyl ether ($2 \times 100 \text{ mL}$). Using a 6 M NaOH solution the aqueous phase was adjusted to pH > 9 and extracted with DCM ($3 \times 150 \text{ mL}$). The combined organic layers were dried over Na_2SO_4 and concentrated. The resulting crude product was purified by flash column chromatography (100% EtOAc) to give 6-benzyloxy-7-methoxyisoquinoline (**4**) as a white solid (1.29 g, 4.88 mmol, 24%). HRMS (EI $^{+}$): 265.1103 calculated for $\text{C}_{17}\text{H}_{15}\text{NO}_2^{+}$ [M] $^{+}$, 265.1110 found. ^1H NMR (400 MHz, CDCl_3): δ (ppm) = 9.04 (s, 1H, 1-H), 8.36 (d, J = 5.6 Hz, 1H, 3-H), 7.51–7.47 (m, 2H, 2'-, 6'-H), 7.44 (d, J = 5.6 Hz, 1H, 4-H), 7.43–7.38 (m, 2H, 3'-, 5'-H), 7.36–7.31 (m, 1H, 4'-H), 7.21 (s, 1H, 8-H), 7.10 (s, 1H, 5-H), 5.29 (s, 2H, CH_2), 4.03 (s, 3H, OCH_3). ^{13}C NMR (101 MHz, CDCl_3): δ (ppm) = 152.3 (C-6), 150.8 (C-7), 150.1 (C-1), 142.1 (C-3), 136.2 (C-1'), 132.5 (C-4a), 128.9 (2C, C-3', 5'), 128.3 (C-4'), 127.4 (2C, C-2', -6'), 125.0 (C-8a), 119.4 (C-4), 106.5 (C-5), 105.7 (C-8), 70.9 (CH_2), 56.2 (OCH_3).

6-Benzyloxy-1-iodo-7-methoxyisoquinoline (5). To a solution of 6-benzyloxy-7-methoxyisoquinoline (**4**) (531 mg, 2.00 mmol) in dry THF (8 mL) was slowly added $\text{TMPMgCl} \cdot \text{LiCl}$ (1.0 M in THF/toluene; 3.00 mL, 3.00 mmol) dropwise at room temperature. After 4 h the reaction mixture was cooled to 0 °C, a solution of iodine (761 mg, 3.00 mmol) in dry THF (3 mL) was added dropwise and the resulting mixture stirred while warming to room temperature over 1 h. Sat. aq. NH_4Cl (4 mL) and sat. aq. $\text{Na}_2\text{S}_2\text{O}_3$ (4 mL) were added and the organic materials extracted using DCM ($3 \times 50 \text{ mL}$). The combined organic layers were dried over Na_2SO_4 and concentrated *in vacuo*. The resulting crude product was purified by flash column chromatography (DCM/EtOAc 5:1) to give 6-benzyloxy-1-iodo-7-

methoxyisoquinoline (**5**) (0.482 g, 1.23 mmol, 62%) as a brown solid. HRMS (EI^{+}): 391.0069 calculated for $C_{17}H_{14}INO_2^{+}$ [M] $^{+}$, 391.0070 found. 1H NMR (400 MHz, $CDCl_3$): δ (ppm) = 8.09 (d, J = 5.4 Hz, 1H, 3-H), 7.50–7.46 (m, 2H, 2'-,6'-H), 7.43–7.34 (m, 5H, 3'-,4'-,5'-, 4-, 8-H), 7.04 (s, 1H, 5-H), 5.30 (s, 2H, CH_2), 4.08 (s, 3H, OCH_3). ^{13}C NMR (101 MHz, $CDCl_3$): δ (ppm) = 152.7 (C-6), 152.0 (C-7), 142.0 (C-3), 135.9 (C-1'), 132.5 (C-1), 128.9 (2C, C-3', -5'), 128.5 (C-4'), 128.3 (C-8a), 127.5 (2C, C-2', -6'), 124.9 (C-4a), 120.3 (C-4), 111.4 (C-8), 106.9 (C-5), 71.1 (CH_2), 56.4 (OCH_3).

6-Benzyloxy-7-methoxy-1-(3,4,5-trimethoxyphenyl)isoquinoline (6). To a solution of 6-benzyloxy-1-iodo-7-methoxyisoquinoline (**5**) (391 mg, 1.00 mmol) in THF (6 mL) was added 3,4,5-trimethoxyphenylboronic acid (254 mg, 1.20 mmol), $Pd(PPh_3)_4$ (59.0 mg, 0.0500 mmol) and aq. K_2CO_3 solution (1.0 M; 3.00 mL, 3.00 mmol). The reaction mixture was stirred in a sealed pressure tube under nitrogen at 90 °C for 16 h. After cooling to room temperature the mixture was poured into water (50 mL) and extracted with EtOAc (3 × 50 mL). The combined organic layers were dried over Na_2SO_4 and concentrated in vacuo. The crude product was purified by flash column chromatography (EtOAc:DCM 2:1) to give 6-benzyloxy-7-methoxy-1-(3,4,5-trimethoxyphenyl)isoquinoline (**6**) (395 mg, 0.915 mmol, 92%) as a yellow solid. HRMS (EI^{+}): 431.1733 calculated for $C_{26}H_{25}NO_5^{+}$ [M] $^{+}$, 431.1729 found. 1H NMR (400 MHz, CD_2Cl_2): δ (ppm) = 8.40 (d, J = 5.5 Hz, 1H, 3-H), 7.52–7.48 (m, 3H, 2'', -6'', -4-H), 7.47 (s, 1H, 8-H), 7.46–7.41 (m, 2H, 3'', -5''-H), 7.40–7.35 (m, 1H, 4''-H), 7.23 (s, 1H, 5-H), 6.93 (s, 2H, 2', -6'-H), 5.24 (s, 2H, CH_2), 3.88 (s, 6H, 3', -5'- OCH_3), 3.87 (s, 3H, 4'- OCH_3), 3.86 (s, 3H, 7'- OCH_3). ^{13}C NMR (101 MHz, CD_2Cl_2): δ (ppm) = 158.5 (C-1), 153.8 (2C, C-3', -5'), 152.4 (C-6), 151.0 (C-7), 141.7 (C-3), 138.8 (C-4'), 136.7 (C-1''), 136.2 (C-1'), 134.2 (C-4a), 129.2 (2C, C-3'', -5''), 128.9 (C-4''), 128.5 (2C, C-2'', -6''), 123.0 (C-8a), 119.2 (C-4), 107.5 (2C, C-2', -6'), 107.0 (C-5), 106.3 (C-8), 71.3 (CH_2), 61.1 (4'- OCH_3), 56.7 (2C, 3', -5'- OCH_3), 56.4 (7'- OCH_3).

7-Methoxy-1-(3,4,5-trimethoxyphenyl)isoquinolin-6-ol (IQTub4). To a solution of 6-benzyloxy-7-methoxy-1-(3,4,5-trimethoxyphenyl)isoquinoline (**6**) (341 mg, 0.790 mmol) in MeOH (30 mL) was added Pd/C (10%, 100 mg). The mixture was stirred vigorously under an atmosphere of hydrogen at room temperature for 24 h, filtered through a pad of celite, and the filtrate concentrated in vacuo to give **IQTub4** (220 mg, 0.645 mmol, 82%) as a white solid. HRMS (EI^{+}): 341.1263 calculated for $C_{19}H_{19}NO_5^{+}$ [M] $^{+}$, 341.1256 found. 1H NMR (400 MHz, $(CD_3)_2SO$): δ (ppm) = 10.29 (s, 1H, OH), 8.31 (d, J = 5.6 Hz, 1H, 3-H), 7.53 (d, J = 5.6 Hz, 1H, 4-H), 7.44 (s, 1H, 8-H), 7.22 (s, 1H, 5-H), 6.99 (s, 2H, 2', -6'-H), 3.84 (s, 6H, 3', -5'- OCH_3), 3.82 (s, 3H, 7'- OCH_3), 3.76 (s, 3H, 4'- OCH_3). ^{13}C NMR (101 MHz, $(CD_3)_2SO$): δ (ppm) = 156.9 (C-1), 152.7 (2C, C-3', -5'), 150.8 (C-6), 149.6 (C-7), 140.4 (C-3), 137.6 (C-4'), 135.3 (C-1'), 133.6 (C-4a), 121.1 (C-8a), 118.1 (C-4), 108.5 (C-5), 107.0 (2C, C-2', -6'), 105.3 (C-8), 60.1 (4'- OCH_3), 56.0 (2C, 3', -5'- OCH_3), 55.4 (7'- OCH_3). HPLC purity: >95%.

Tubulin Polymerisation in vitro assay. 99% purity tubulin from porcine brain was used in polymerisation assays run according to manufacturer's instructions (Cytoskeleton Inc., cat. #T240). Tubulin was pre-incubated for 10 min at 37 °C with either **IQTub5** (20 μ M) or colchicine (16 μ M) (in buffer (with 3% DMSO, 10% glycerol) as appropriate; at time zero, GTP (1 mM) was added and the absorbance at 340 nm was monitored over time at 37 °C [44].

Cell Culture. HeLa cells were maintained under standard cell culture conditions in Dulbecco's modified Eagle's medium supplemented with 10% fetal calf serum (FCS), 100 U/mL penicillin and 100 U/mL streptomycin, at 37 °C in a 5% CO_2 atmosphere. HL-60 cells were cultured in RPMI 1640 medium with 10% FCS without antibiotics at 37 °C in a 5% CO_2 atmosphere. Compounds and cosolvent (DMSO; 1% final concentration) were added via a D300e digital dispenser (Tecan).

Antiproliferation Assays. Mitochondrial diaphorase activity in HeLa cell line was quantified by spectrophotometrically measuring the reduction of resazurin (7-hydroxy-3H-phenoxazin-3-one-10-oxide) to resorufin. 5,000 cells/well were seeded on 96-well microtitre plates and treated with **IQTubs** 24 h later. Following 48 h of treatment, cells were incubated with 20 μ L of 0.15 mg/mL resazurin per well for 3 h at 37 °C. The resorufin fluorescence (excitation 544 nm, emission 590 nm) was then measured.

HL-60 cells were seeded in 96-well plates at 9,000 cells/well and incubated for 24 h before treatment with **IQTubs**. 24 h later, cells were treated with 0.5 mg/mL (3-(4,5-dimethylthiazol-2-yl)-2,5-diphenyltetrazolium bromide (MTT) for 2 h; the medium was aspirated and formazan crystals were re-dissolved in DMSO (190 μ L) to measure their absorbance at 570 nm.

Fluorescence and absorbance were measured on a FLUOstar Omega microplate reader (BMG Labtech), averaged over the technical replicates and normalised as viability by reference to the cosolvent-only control set as 100%, and to cell-free (resazurin) or Triton-X®-100-treated (MTT) controls set as 0%. Results are means of at least three independent experiments.

Cell cycle analysis. **IQTubs** were added to HeLa cells in 24-well plates (seeding density: 50,000 cells/well) and incubated for 24 h. Cells were collected and stained with 2 μ g/mL propidium iodide (PI) at 4 °C for 30 min. Following PI staining, cells were analysed by flow cytometry using a BD LSR Fortessa flow cytometer (Becton Dickinson) run by BD FACSDiva software. 30,000 cells were measured per condition and the data were transferred to Flowing software for cell cycle analysis. Cells were sorted into sub-G1, G1, S and G2/M phase according to DNA content (PI signal).

Immunofluorescence staining. HeLa cells seeded on glass coverslips in 24-well plates (50,000 cells/well) were left to adhere for 18 h then treated for 24 h with **IQTubs**. Cover slips were washed then fixed with 0.5% glutaraldehyde, quenched with 0.1% $NaBH_4$, blocked with PBS + 10% FCS, and treated with rabbit alpha-tubulin primary antibody (Abcam ab18251; 1:400 in PBS + 10% FCS) for 1 h; after washing with PBS, cells were incubated with goat-anti-rabbit Alexa fluor 488 secondary antibody (Abcam, ab150077; 1:400 in PBS + 10% FCS) for 1 h. After washing with PBS, coverslips were mounted onto glass slides using Roti-Mount FluorCare DAPI (Roth) and imaged with a Zeiss LSM Meta confocal microscope. Images were processed using Fiji software. For maximum intensity projections, images were recorded at different focal planes by incrementally stepping through the sample (step size 1–2 μ m) and maximum intensity projections were obtained using Fiji.

EB3 comet assay. [45] HeLa cells (12,000 cells/well) were seeded on 8-well ibiTreat μ slides (ibidi) 24 h prior to transfection. Cells were transiently transfected with EB3-YFP plasmid using jetPRIME reagent (Polyplus) according to the manufacturer's instructions. Cells were imaged 24 h later, under 37 °C and 5% CO_2 atmosphere using an UltraVIEW Vox spinning disc confocal microscope (PerkinElmer) equipped with an EMCCD camera (Hamamatsu, Japan) and operated with Volocity software. After focussing on cells on the microscope stage, 5 imaging frames were acquired to set a reference measure for EB3 comet activity, then **IQTub4P** was added cautiously and cells incubated for 2 min before acquiring another 5 frames to quantify post-treatment EB3 comet activity. Cells were imaged at 514 nm (20% laser power, 300 ms exposure time, 45 frames/min). For EB3 comet statistics, 7 cells from three independent trials were taken. EB3 comets were counted with a Fiji plugin based on the "Find maxima" function from the NIH.

Author contributions

Y.K. performed immunofluorescence staining, live-cell microscopy and viability studies. C.G. performed synthesis and

coordinated chemical data assembly. B.M. and L.G. performed synthesis. C.H. and M.P. performed cell cycle analysis and viability studies. J.A. supervised biology, performed cell cycle analysis and viability studies, and coordinated biological data assembly. F.B. planned and supervised synthesis. O.T.-S. designed the study, supervised synthesis and biology, coordinated data assembly and wrote the manuscript.

Declaration of competing interest

The authors declare no conflict of interest.

Acknowledgments

This research was supported by funds from the German Research Foundation (DFG): SFB1032 Nanoagents for Spatiotemporal Control project B09 to O.T.-S.; SFB TRR 152 project P24 number 239283807 to O.T.-S.; and Emmy Noether grant to O.T.-S.) and the German Ministry of Education and Research (GO-Bio grant to O.T.-S.). We thank Rebekkah Bingham (LMU) for performing the tubulin polymerisation assay, Yuliia Holota (Bienta) for the *in vitro* ADME and *in vivo* tolerated dose assessments, Martina Stadler (LMU) for the HL-60 viability crosscheck, K. T. Wanner (LMU) for kind support and collegial discussions, and H. Harz and I. Solvei (LMU microscopy platform CALM) for microscopy support.

Appendix A. Supplementary data

Supplementary data to this article can be found online at <https://doi.org/10.1016/j.ejmech.2019.111865>.

References

- [1] T.J. Mitchison, The proliferation rate paradox in antimetabolic chemotherapy, *Mol. Biol. Cell* 23 (1) (2012) 1–6, <https://doi.org/10.1091/mbc.e10-04-0335>.
- [2] J.R. Peterson, T.J. Mitchison, Small molecules, big impact: a history of chemical inhibitors and the cytoskeleton, *Chem. Biol.* 9 (12) (2002) 1275–1285, [https://doi.org/10.1016/s1074-5521\(02\)00284-3](https://doi.org/10.1016/s1074-5521(02)00284-3).
- [3] D.G.I. Kingston, Taxol, a molecule for all seasons, *Chem. Commun.* 10 (2001) 867–880, <https://doi.org/10.1039/b100070p>.
- [4] D.W. Siemann, The unique characteristics of tumor vasculature and preclinical evidence for its selective disruption by tumor-vascular disrupting agents, *Cancer Treat. Rev.* 37 (1) (2011) 63–74, <https://doi.org/10.1016/j.ctrv.2010.05.001>.
- [5] G.M. Tozer, C. Kanthou, B.C. Baguley, Disrupting tumour blood vessels, *Nat. Rev. Cancer* 5 (6) (2005) 423–435, <https://doi.org/10.1038/nrc1628>.
- [6] K.G. Pinney, Molecular recognition of the colchicine binding site as a design paradigm for the discovery and development of vascular disrupting agents, in: *Vascular-Targeted Therapies in Oncology*, Wiley, 2006, pp. 95–121.
- [7] T.L. Nguyen, C. McGrath, A.R. Hermone, J.C. Burnett, D.W. Zaharevitz, B.W. Day, P. Wipf, E. Hamel, R. Gussio, A common pharmacophore for a diverse set of colchicine site inhibitors using a structure-based approach, *J. Med. Chem.* 48 (19) (2005) 6107–6116, <https://doi.org/10.1021/jm050502t>.
- [8] R. Gaspari, A.E. Prota, K. Bargsten, A. Cavalli, M.O. Steinmetz, Structural basis of *cis*- and *trans*-combretastatin binding to tubulin, *Chem* 2 (1) (2017) 102–113, <https://doi.org/10.1016/j.chempr.2016.12.005>.
- [9] M. Borowiak, W. Nahaboo, M. Reynders, K. Nekolla, P. Jalinet, J. Hasserodt, M. Rehberg, M. Delattre, S. Zahler, A. Vollmar, et al., Photoswitchable inhibitors of microtubule dynamics optically control mitosis and cell death, *Cell* 162 (2) (2015) 403–411, <https://doi.org/10.1016/j.cell.2015.06.049>.
- [10] G.R. Pettit, S.B. Singh, E. Hamel, C.M. Lin, D.S. Alberts, D. Garcia-Kendal, Isolation and structure of the strong cell growth and tubulin inhibitor combretastatin A-4, *Experientia* 45 (2) (1989) 209–211, <https://doi.org/10.1007/bf01954881>.
- [11] J.A. Woods, J.A. Hadfield, G.R. Pettit, B.W. Fox, A.T. McGown, The interaction with tubulin of a series of stilbenes based on combretastatin A-4, *Br. J. Canc.* 71 (4) (1995) 705–711, <https://doi.org/10.1038/bjc.1995.138>.
- [12] G.M. Tozer, C. Kanthou, C.S. Parkins, S.A. Hill, The biology of the combretastatins as tumour vascular targeting agents, *Int. J. Exp. Pathol.* 83 (1) (2002) 21–38, <https://doi.org/10.1046/j.1365-2613.2002.00211.x>.
- [13] G.C. Tron, T. Pirali, G. Sorba, F. Pagliai, S. Busacca, A.A. Genazzani, Medicinal chemistry of combretastatin A4: present and future directions, *J. Med. Chem.* 49 (11) (2006) 3033–3044, <https://doi.org/10.1021/jm0512903>.
- [14] D. Tarade, D. Ma, C. Pignanelli, F. Mansour, D. Simard, S. van den Berg, J. Gauld, J. McNulty, S. Pandey, Structurally simplified biphenyl combretastatin A4 derivatives retain *in vitro* anti-cancer activity dependent on mitotic arrest, *PLoS One* 12 (3) (2017), e0171806, <https://doi.org/10.1371/journal.pone.0171806>.
- [15] J. McNulty, S. van den Berg, D. Ma, D. Tarade, S. Joshi, J. Church, S. Pandey, Antimitotic activity of structurally simplified biaryl analogs of the anticancer agents colchicine and combretastatin A4, *Bioorg. Med. Chem. Lett.* 25 (1) (2015) 117–121, <https://doi.org/10.1016/j.bmcl.2014.10.090>.
- [16] S. Kim, H. Ko, J.E. Park, S. Jung, S.K. Lee, Y.-J. Chun, Design, synthesis, and discovery of novel *trans*-stilbene analogues as potent and selective human cytochrome P450 1B1 inhibitors, *J. Med. Chem.* 45 (1) (2002) 160–164, <https://doi.org/10.1021/jm010298j>.
- [17] D.-J. Hwang, J. Wang, W. Li, D.D. Miller, Structural optimization of indole derivatives acting as colchicine binding site as potential anticancer agents, *ACS Med. Chem. Lett.* 6 (9) (2015) 993–997, <https://doi.org/10.1021/acsmchemlett.5b00208>.
- [18] Y. Lu, J. Chen, J. Wang, C.-M. Li, S. Ahn, C.M. Barrett, J.T. Dalton, W. Li, D.D. Miller, Design, synthesis, and biological evaluation of stable colchicine binding site tubulin inhibitors as potential anticancer agents, *J. Med. Chem.* 57 (17) (2014) 7355–7366, <https://doi.org/10.1021/jm500764v>.
- [19] S.A. Hill, G.M. Tozer, G.R. Pettit, D.J. Chaplin, Preclinical evaluation of the antitumour activity of the novel vascular targeting agent oxi 4503, *Anticancer Res.* 22 (3) (2002) 1453–1458.
- [20] Y. Nihei, M. Suzuki, A. Okano, T. Tsuji, Y. Akiyama, T. Tsuruo, S. Saito, K. Hori, Y. Sato, Evaluation of antivasculature and antimitotic effects of tubulin binding agents in solid tumor therapy, *Jpn. J. Cancer Res.* 90 (12) (1999) 1387–1395, <https://doi.org/10.1111/j.1349-7006.1999.tb00724.x>.
- [21] P.D. Davis, G.J. Dougherty, D.C. Blakey, S.M. Galbraith, G.M. Tozer, A.L. Holder, M.A. Naylor, J. Nolan, M.R.L. Stratford, D.J. Chaplin, et al., ZD6126: a novel vascular-targeting agent that causes selective destruction of tumor vasculature, *Cancer Res.* 62 (24) (2002) 7247–7253.
- [22] G. Kremmidiotis, A.F. Leske, T.C. Lavanros, D. Beaumont, J. Gasic, A. Hall, M. O'Callaghan, C.A. Matthews, B. Flynn, BNC105: a novel tubulin polymerization inhibitor that selectively disrupts tumor vasculature and displays single-agent antitumor efficacy, *Mol. Cancer Ther.* 9 (6) (2010) 1562, <https://doi.org/10.1158/1535-7163.mct-09-0815>.
- [23] R.P. Mason, D. Zhao, L. Liu, M.L. Trawick, K.G. Pinney, A perspective on vascular disrupting agents that interact with tubulin: preclinical tumor imaging and biological assessment, *Integr. Biol. (Camb)* 3 (4) (2011) 375–387, <https://doi.org/10.1039/c0ib00135j>.
- [24] J.H. Gill, K.L. Rockley, C. De Santis, A.K. Mohamed, Vascular disrupting agents in cancer treatment: cardiovascular toxicity and implications for co-administration with other cancer chemotherapeutics, *Pharmacol. Ther.* 202 (2019) 18–31, <https://doi.org/10.1016/j.pharmthera.2019.06.001>.
- [25] P. Giannakakou, D. Sackett, T. Fojo, Tubulin/microtubules: still a promising target for new chemotherapeutic agents, *J. Natl. Cancer Inst.* 92 (3) (2000) 182–183, <https://doi.org/10.1093/jnci/92.3.182>.
- [26] O. Thorn-Seshold, F. Bracher, B. Melzer, Isoquinoline Biaryl Compounds, 2018. EP18207030.
- [27] M. Sriram, J.J. Hall, N.C. Grohmann, T.E. Strecker, T. Wootton, A. Franken, M.L. Trawick, K.G. Pinney, Design, synthesis and biological evaluation of dihydronaphthalene and benzosuberene analogs of the combretastatins as inhibitors of tubulin polymerization in cancer chemotherapy, *Bioorg. Med. Chem.* 16 (17) (2008) 8161–8171, <https://doi.org/10.1016/j.bmc.2008.07.050>.
- [28] Y. Pang, H. Lin, C. Ou, Y. Cao, B. An, J. Yan, X. Li, Design, synthesis, and biological evaluation of novel benzodiazepine derivatives as anticancer agents through inhibition of tubulin polymerization *in vitro* and *in vivo*, *Eur. J. Med. Chem.* 182 (2019) 111670, <https://doi.org/10.1016/j.ejmech.2019.111670>.
- [29] Verfahren Zur Darstellung von 1- (3, 4, 5-Trialkoxyphenyl)-6, 7-Dialkoxyisochinolininen. DE614703.
- [30] W. Reeve, W.M. Eareckson, Synthesis of some isoquinoline derivatives related to podophylotoxin, *J. Am. Chem. Soc.* 72 (11) (1950) 5195–5197, <https://doi.org/10.1021/ja01167a114>.
- [31] B. Melzer, F. Bracher, A divergent approach to benzyloisoquinoline-type and oxoaporphine alkaloids via regioselective direct ring metalation of alkoxy isoquinolines, *Org. Biomol. Chem.* 13 (28) (2015) 7664–7672, <https://doi.org/10.1039/c5ob00926j>.
- [32] B. Melzer, F. Bracher, A novel approach to oxoisoaporphine alkaloids via regioselective metalation of alkoxy isoquinolines, *Beilstein J. Org. Chem.* 13 (2017) 1564–1571, <https://doi.org/10.3762/bjoc.13.156>.
- [33] A. Sailer, F. Ermer, Y. Kraus, F. Lutter, C. Donau, M. Bremerich, J. Ahlfeld, O. Thorn-Seshold, Hemithioindigos as desymmetrised molecular switch scaffolds: design control over the isomer-dependency of potent photoswitchable antimetabolic bioactivity in cellulose, *Chembiochem* 20 (2019) 1305–1314, <https://doi.org/10.1002/cbic.201800752>.
- [34] L. Gao, Y. Kraus, M. Wranik, T. Weinert, S.D. Pritzl, J.C.M. Meiring, R. Bingham, N. Olieric, A. Akhmanova, T. Lohmüller, et al., Photoswitchable microtubule inhibitors enabling robust, GFP-orthogonal optical control over the tubulin cytoskeleton, 2019, p. 716233, <https://doi.org/10.1101/716233>. bioRxiv 2019.
- [35] A. Sailer, F. Ermer, Y. Kraus, R. Bingham, F.H. Lutter, J. Ahlfeld, O. Thorn-Seshold, Potent Hemithioindigo-Based Antimitotics Photocontrol the Microtubule Cytoskeleton in Cellulo, *ChemRxiv*, 2019. <https://doi.org/10.26434/chemrxiv.9176747.v1>.
- [36] K.G. Pinney, G.R. Pettit, M.L. Trawick, C. Jelinek, D.J. Chaplin, The discovery and development of the combretastatins, in: *Anticancer Agents from Natural Products*, CRC Press, Boca Raton, 2011, pp. 27–63.

- [37] National Cancer Institute, NCI Drug Dictionary: fosbretabulin disodium. <https://www.cancer.gov/publications/dictionaries/cancer-drug/def/fosbretabulin-disodium>.
- [38] E. Reimann, H. Renz, Protoberberine Aus Reissert-Verbindungen, 2. Mitt.: eine Neue Synthese von 8-Methyldibenzo[a,g]Chinolizidinen, Arch. Pharm. 326 (5) (1993) 253–258, <https://doi.org/10.1002/ardp.19933260502>.
- [39] A. Krasovskiy, V. Krasovskaya, P. Knochel, Mixed Mg/Li amides of the type $R_2NMgCl \cdot LiCl$ as highly efficient bases for the regioselective generation of functionalized aryl and heteroaryl magnesium compounds, Angew. Chem. Int. Ed. 45 (18) (2006) 2958–2961, <https://doi.org/10.1002/anie.200504024>.
- [40] T.L. Riss, A.L. Niles, R.A. Moravec, Cell Viability Assays, 2013 May 1 [Updated 2016 Jul 1], <https://www.ncbi.nlm.nih.gov/books/NBK144065/>. (Accessed 8 May 2019).
- [41] M.J. Waring, Defining optimum lipophilicity and molecular weight ranges for drug candidates—molecular weight dependent lower LogD limits based on permeability, Bioorg. Med. Chem. Lett 19 (10) (2009) 2844–2851, <https://doi.org/10.1016/j.bmcl.2009.03.109>.
- [42] K.A. Monk, R. Siles, M.B. Hadimani, B.E. Mugabe, J.F. Ackley, S.W. Studerus, K. Edvardsen, M.L. Trawick, C.M. Garner, M.R. Rhodes, et al., Design, synthesis, and biological evaluation of combretastatin nitrogen-containing derivatives as inhibitors of tubulin assembly and vascular disrupting agents, Bioorg. Med. Chem. 14 (9) (2006) 3231–3244, <https://doi.org/10.1016/j.bmc.2005.12.033>.
- [43] A.R. Battersby, D.J. Le Count, S. Garratt, R.I. Thrift, Synthetic applications of 1,2-dihydroisoquinolines: synthesis of (\pm)-Coreximine, Tetrahedron 14 (1) (1961) 46–53, [https://doi.org/10.1016/0040-4020\(61\)80086-0](https://doi.org/10.1016/0040-4020(61)80086-0).
- [44] C.M. Lin, S.B. Singh, P.S. Chu, R.O. Dempcy, J.M. Schmidt, G.R. Pettit, E. Hamel, Interactions of tubulin with potent natural and synthetic analogs of the antimitotic agent combretastatin: a structure-activity study, Mol. Pharmacol. 34 (2) (1988) 200–208.
- [45] T. Kleele, P. Marinković, P.R. Williams, S. Stern, E.E. Weigand, P. Engerer, R. Naumann, J. Hartmann, R.M. Karl, F. Bradke, et al., An assay to image neuronal microtubule dynamics in mice, Nat. Commun. 5 (2014) 4827, <https://doi.org/10.1038/ncomms5827>.